Advanced diffusion imaging of abdominal organs in different hydration states of the human body: stability of biomarkers

Kemėšienė, Jūratė ; Rühle, Alexander ; Gomolka, Ryszard ; Wurnig, Moritz C ; Rossi, Cristina ; Boss, Andreas

Abstract: Background MR diffusion weighted imaging (DWI) may provide important information regarding the pathophysiology of parenchymal abdominal organs. The purpose of our study was to investigate the stability of imaging biomarkers of diffusion weighted imaging (DWI), intravoxel incoherent motion (IVIM) and diffusion kurtosis imaging (DKI) in abdominal parenchymal organs regarding two body hydration states. Methods Ten healthy volunteers twice underwent DWI of abdominal organs using a double-refocused spin-echo echo-planar imaging sequences with 11 different b-values (ranging from 0 to 1,500 s/mm^2): after 4 h of fluid deprivation; 45 min following 1000 ml of water intake. Four different diffusion models were evaluated and compared: standard DWI, DKI with mono-exponential fitting, multistep algorithm with variable b-value threshold for IVIM, combined IVIM-Kurtosis; in four abdominal organs: kidneys, liver, spleen and psoas muscle. Results Diffusion parameters from all four models remained similar for the renal parenchyma before and after the water challenge. Significant differences were found for the liver, spleen, and psoas muscle. The largest effects were seen for: the liver parenchyma after the water challenge by means of IVIM model's true diffusion ($p < 0.02$); the spleen, for IVIM's perfusion fraction ($p < 0.03$), the psoas muscle for the ADC value ($p < 0.02$). Conclusions Herein, we showed that diffusion parameters of the kidney remain remarkably stable regarding the hydration status. This may be attributed to the kidney-specific compensatory mechanisms. For the liver, spleen and psoas muscle the diffusion parameters were sensitive to changes of the hydration. This phenomenon needs to be considered when evaluating diffusion data of these organs.

DOI: https://doi.org/10.1016/j.heliyon.2021.e06072

DOI: https://doi.org/10.1016/j.heliyon.2021.e06072

Heliyon 7 (2021) e06072

Contents lists available at ScienceDirect

Heliyon

journal homepage: www.cell.com/heliyon

Research article

Advanced diffusion imaging of abdominal organs in different hydration states of the human body: stability of biomarkers

Jūratė Kemėšienė [a,*], Alexander Rühle [b], Ryszard Gomolka [c], Moritz C. Wurnig [c], Cristina Rossi [c], Andreas Boss [c]

[a] Department of Radiology, Hospital of Lithuanian University of Health Sciences, Kaunas Clinics, Lithuania
[b] Department of Molecular Radiation Oncology, German Cancer Research Center (dkfz), Heidelberg, Germany
[c] Institute of Diagnostic and Interventional Radiology, University Hospital Zurich, Switzerland

ARTICLE INFO

Keywords:
Magnetic resonance
Diffusion
Kurtosis
Tissue hydration

ABSTRACT

Background: MR diffusion weighted imaging (DWI) may provide important information regarding the pathophysiology of parenchymal abdominal organs. The purpose of our study was to investigate the stability of imaging biomarkers of diffusion weighted imaging (DWI), intravoxel incoherent motion (IVIM) and diffusion kurtosis imaging (DKI) in abdominal parenchymal organs regarding two body hydration states.

Methods: Ten healthy volunteers twice underwent DWI of abdominal organs using a double-refocused spin-echo echo-planar imaging sequences with 11 different b-values (ranging from 0 to 1,500 s/mm^2): after 4 h of fluid deprivation; 45 min following 1000 ml of water intake. Four different diffusion models were evaluated and compared: standard DWI, DKI with mono-exponential fitting, multistep algorithm with variable b-value threshold for IVIM, combined IVIM-Kurtosis; in four abdominal organs: kidneys, liver, spleen and psoas muscle.

Results: Diffusion parameters from all four models remained similar for the renal parenchyma before and after the water challenge. Significant differences were found for the liver, spleen, and psoas muscle. The largest effects were seen for: the liver parenchyma after the water challenge by means of IVIM model's true diffusion ($p < 0.02$); the spleen, for IVIM's perfusion fraction ($p < 0.03$), the psoas muscle for the ADC value ($p < 0.02$).

Conclusions: Herein, we showed that diffusion parameters of the kidney remain remarkably stable regarding the hydration status. This may be attributed to the kidney-specific compensatory mechanisms. For the liver, spleen and psoas muscle the diffusion parameters were sensitive to changes of the hydration. This phenomenon needs to be considered when evaluating diffusion data of these organs.

1. Introduction

MR diffusion weighted imaging (DWI) may provide important information regarding the pathophysiology of parenchymal abdominal organs. In DWI, diffusion gradients are applied to measure the degree of water motion, which in the most simple model is quantified by the Apparent Diffusion Coefficient (ADC, in mm^2/s) assuming a mono-exponential signal pattern [1, 2]. Hence, it was demonstrated that in the kidneys, DWI allows a quantitative assessment of the degree of interstitial fibrosis in chronic kidney disease or acute graft rejection after kidney transplantation [3]. However, diffusion measurements may also be affected by intravoxel incoherent fluid movements [4, 5, 6]. A model taking into account these effects, called intravoxel incoherent motion (IVIM), was proposed by applying a bi-exponential approach for improvement of diffusion signal evaluation particularly at low b-values [7]. IVIM analysis can be used to investigate the underlying tissue microstructure and intra-voxel pseudo-diffusive fluid regimes by assessment of two diffusion components: molecular water diffusion in the tissue and water motion mostly affected by perfusion in microcirculation and often described as pseudodiffusion [4, 8]. Several studies showed that IVIM is sensitive to pathological processes in kidneys, such as allograft rejection, various renal tumors, renal artery stenosis or renal dysfunction [3, 9] as well as the hydration level and caloric intake [9, 10, 11].

Diffusion kurtosis imaging (DKI) is another model derived from conventional DWI, which requires ultrahigh b-values (>1000 s/m^2) and a modification of the mono-exponential curve-fitting approach. The conventional DWI model is based on the assumption that water diffusion

* Corresponding author.
E-mail addresses: jurate.did@gmail.com, juradidz1012@kmu.lt (J. Kemėšienė).

https://doi.org/10.1016/j.heliyon.2021.e06072
Received 1 March 2020; Received in revised form 24 July 2020; Accepted 20 January 2021

follows a Gaussian motion behaviour without restriction. DKI provides complementary information on the microstructural complexity of the tissue by evaluating the non-Gaussian behaviour of water motion. Hence, DKI analysis is associated with two variables: *K*, which quantifies the deviation of water diffusion from a Gaussian pattern, and *D*, which is the diffusion coefficient corrected by a non-Gaussian bias [12, 13].

Advanced diffusion methods such as IVIM and diffusion kurtosis may have potential for detection, staging and evaluation of the progression of various liver diseases, such as fibrosis and cirrhosis as well as in the characterization of focal liver lesions [19, 20]. It was previously shown that portal venous flow increases 30 min after food intake, and the diffusion parameters obtained between fasting and food intake change less than 10% without reaching statistical significance.

Herein, we aimed to investigate whether diffusion markers derived from different diffusion models are sensitive to the hydration state, based on measurements in abdominal organs of 10 healthy volunteers, in normal condition and subjected to 1000ml water challenge. The diffusion markers were evaluated and compared in four abdominal organs: kidneys, liver, spleen and psoas muscle; using four different diffusion models: conventional mono-exponential DWI, DKI, IVIM and combined IVIM-DKI.

2. Methods

2.1. Subjects and protocol

The current study was approved by the local Ethics Committee and included 10 healthy young volunteers (4 male) of age between 24 and 33 years. All volunteers gave their written informed consent to the MR examination and the following scientific evaluation of the acquired data. To standardize the hydration state, all volunteers refrained from in-taking of any fluids within 4 h before the first MRI scanning. After the first MRI acquisition, volunteers were intraorally administered with 1,000 ml of water. To optimize the water absorption in the gastrointestinal tract, volunteers were asked to remain in vertical position and subsequently underwent the second MRI acquisition performed 45 min after the water administration.

2.2. MRI examinations

MR imaging was performed by means of a clinical 3T MR scanner (MAGNETOM Skyra, Siemens Healthcare, Erlangen, Germany) using an 18-channel flexible anterior phased-array coil and built-in posterior spine coil. The MRI protocol consisted of T2-weighted morphological scans using multi breath-hold T2 half Fourier single-shot turbo spin-echo (HASTE: TR/TE = 1370/112 ms; flip angle = 129°; bandwidth = 445 Hz/px; voxel size = 1.2 × 1.2 × 5 mm^3; FOV = 384 × 384 mm^2) for anatomical reference, and DWI using a spin-echo with twice-refocused diffusion preparation echo-planar imaging (EPI) sequence in coronal orientation during free breathing. (TR/TE = 3500/82 ms; flip angle = 90° bandwidth = 2170 Hz/px; voxel size = 3 × 3 × 5 mm^3; FOV = 384 × 384 mm^2, number of slices 12, slice gap 20%, acquisition time 4min 44sec) was acquired with 11 consecutive b-values (number of spatial averages at b-value): 0, 10 (2), 40 (2), 90 (2), 170 (2), 240 (2), 390 (3), 750 (4), 1000 (4), as proposed by Lemke et al. (8). Additional b = values of 1250 (5) and 1500 (5) s/mm^2 were added for DKI analysis. Diffusion-encoding gradients were aligned along three orthogonal directions.

2.3. ROI definition

For subsequent DWI signal curve-fitting, regions of interest (ROI) were manually drawn over the five different body regions in b-0 image, for every subject separately. ROIs were manually defined for: the renal parenchyma of both kidneys in the slice covering the hilum; the liver in the slice covering its largest coronal section; the middle section of the spleen in the slice covering the hilum; the middle section of the right major psoas muscle. Subsequently, the ROIs were copied to the images of higher b-values to depict the mean DWI signal from every ROI separately, in every DWI image (Figure 1). All signal intensity curves were normalized to the b = 0 s/mm^2 image before curve fitting to allow a better visualization of the curve behaviour of the individual curves.

2.4. Post-processing and curve fitting

All post-processing was performed using in-house computer scripts in Matlab 2016b (The Mathworks, Nattick, MA, USA). Exponential curve fitting was performed using the Levenberg-Marquardt algorithm. The ADC values were quantified by mono-exponential curve fitting to the measured mean signal intensities within ROIs from all 11 b-values:

$$S(b) = S(0) \cdot e^{-bADC} \quad (1)$$

where ***S(b)*** represents the mean signal intensity within the ROI from the DWI image acquired at the *b*-value ***b***, ***S(0)*** is the signal intensity at *b* = 0 s/mm^2, and ADC is the Apparent Diffusion Coefficient.

For high b-values (>1000 s/m^2), the non-Gaussian diffusion due to barriers in the microarchitecture of the tissue causes deviations from the standard DWI model. For the curve fitting of the DKI model, the following equation was applied:

$$S(b) = S(0) \cdot e^{-bD+b^2D^2\frac{K}{6}} \quad (2)$$

where ***D*** is the diffusion coefficient of "pure" molecular water diffusion and ***K*** – the kurtosis value.

Since DWI data includes influences from microcirculation particularly for low b-values, a bi-exponential IVIM model is used to separate diffusion from perfusion effects:

$$S(b) = S(0) \cdot \left(F_p \cdot e^{-bD^*} + \left(1 - F_p\right) \cdot e^{-bD}\right) \quad (3)$$

where $\boldsymbol{F_p}$ is the perfusion fraction and $\boldsymbol{D^*}$ the pseudodiffusion coefficient.

Finally, we combined both IVIM and DKI models using the following equation:

$$S(b) = S(0) \cdot \left(F_p \cdot e^{-bD^*} + \left(1 - F_p\right) \cdot e^{-bD+b^2D^2\frac{K}{6}}\right) \quad (4)$$

To overcome the need of choice of an appropriate threshold and to minimize numerical errors during calculation a step-wise parameter-free

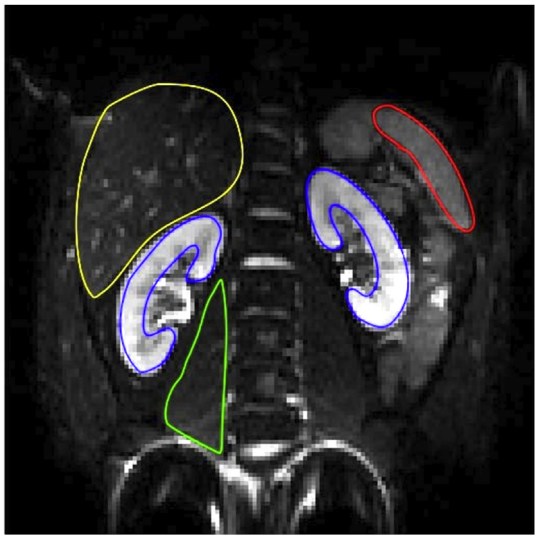

Figure 1. Typical ROI placement for: a) right kidney cortex (blue), b) left kidney cortex (blue), c) liver (yellow), d) spleen (red), e) psoas muscle (green).

algorithm was used for the last two models (Eqs. (3) and (4)), as proposed by Wurnig et al. [14, 15]. For all above described models, curve fitting was performed using all 11 b-values accepting e.g. the known influences of low-b-values on mono-exponential fitting to obtain the ADC, which was done to avoid an arbitrary choice of b-values for particular diffusion models. Regarding the combined IVIM and kurtosis model, IVIM parameters were evaluated first with subsequent evaluation of kurtosis parameters in the step-wise approach, which resulted in higher stability of parameters.

2.5. Statistical evaluation

All statistical analyses were performed using GraphPad Prism (ver. 5.04, GraphPad Software, La Jolla, CA, USA). For all diffusion parameters estimated by means of Eqs. (1), (2), (3), and (4), for each organ, their mean and standard deviation (SD) values were computed for each subject. The Shapiro-Wilk normality test was applied to check the normality of the mean values calculated from each subject separately. Subsequently, the paired two-tailed two sample Student's *t*-test was applied to compare the values obtained before and after water challenge, for different organs diffusion model-wise. All results were considered significant for $p < 0.05$ with no correction applied for multiple comparisons (Table 1).

3. Results

3.1. MRI examinations

All MRI scans were of sufficient image quality for scientific data evaluation and no significant motion or breathing artefacts were visible. Typical signal intensity curves for the renal, liver and the spleen parenchyma and the right psoas are shown in Figures 2, 3, and 4. The liver and the spleen parenchyma showed a rapid drop of signal intensity for low b-values indicating a large contribution of perfusion effects, whereas the renal parenchyma and psoas muscle exhibited a more gradual decrease of signal intensities at low b-values.

3.2. Diffusion curve fitting and analysis

The conventional DWI model insufficiently described signal patterns in organs with large perfusion effects at low-b-values, with marked deviation of the fitting curve from the measurement points. The DKI model

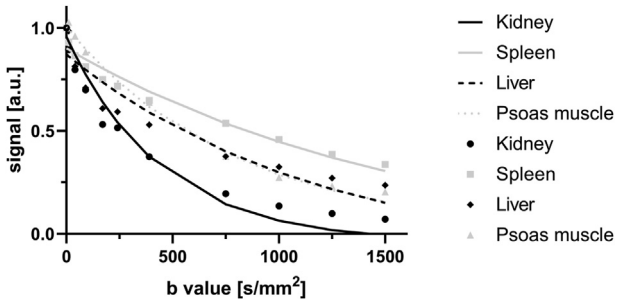

Figure 2. Typical DWI fitting curves before water challenge for kidney cortex, liver, spleen and psoas muscle. The figure represents the DWI values of one volunteer.

exhibited deviations especially in high b-values with an up-slope of the fitting curve in all assessed organs (not graphically displayed). IVIM and IVIM-DKI models, both including IVIM effects provided a good description of the signal curves without relevant deviations from the measurement points (Figure 3). A superposition of the fitting curves using the IVIM-DKI model is displayed in Figure 4.

Mean values of the parameters calculated by means of four different diffusion models for each evaluated organ are presented in Table 1. Highest water diffusion was consistently found in the renal parenchyma, whereas lowest ADC and D values were seen in the liver and the spleen. Pseudodiffusion D* values obtained with the IVIM and IVIM-DKI models before and after water challenge were highest for the liver (before water challenge – D*_IVIM: 54.89 ± 35.74 × 10^{-3} mm^2/s, D*_IVIM_DKI: 72.17 ± 48,86 × 10^{-3} mm^2/s; after water challenge – D*_IVIM: 99.74 ± 70.89 × 10^{-3} mm^2/s, D*_IVIM_DKI: 136.13 ± 88.98 × 10^{-3} mm^2/s), whereas the perfusion fraction values, using IVIM model before and after water challenge were highest in the renal parenchyma (before water challenge – Fp_IVIM: 0.37–0.39 × 10^{-3} mm^2/s; after water challenge – Fp_IVIM: 0.36–0.43 × 10^{-3} mm^2/s) and the liver (before water challenge – Fp_IVIM: 0.33 ± 0.09 × 10^{-3} mm^2/s; after water challenge – Fp_IVIM: 0.28–0.12 × 10^{-3} mm^2/s). The liver also showed the highest perfusion fraction values using IVIM-DKI model before and after water challenge (before water challenge – Fp_IVIM_DKI: 0.27 ± 0.12 × 10^{-3} mm^2/s; after water challenge – Fp_IVIM_DKI: 0.31 ± 0.23 × 10^{-3} mm^2/s;). DKI before and after water challenge showed the highest calculated *K* value for the spleen (before water challenge –K_DKI: 1.31 ± 0.39 × 10^{-3} mm^2/s; after water challenge – K_DKI: 0.13 ± 0.86 × 10^{-3} mm^2/s;).

Table 1. Means ± standard deviations of the diffusion parameters calculated from conventional DWI, intravoxel incoherent motion (IVIM), diffusion kurtosis (DKI) and combined IVIM-DKI imaging models before (B/w) and after (A/w) water administration, among n = 10 healthy subjects.

	Left kidney		Right kidney		Liver		Spleen		Psoas muscle	
	B/w	A/w	B/w	A/w	B/w	A/w	B/w	A/w	B/w	A/w
Model 1 (DWI)										
ADC (10^{-3} mm^2/s)	2.37 ± 0.45	2.21 ± 0.21	2.56 ± 1.06	2.21 ± 0.22	1.31 ± 0.21	1.35 ± 0.18	1.25 ± 1.63	0.73 ± 0.04	1.16 ± 0.14	**1.25 ± 0.12***
Model 2 (DKI)										
D (10^{-3} mm^2/s)	3.22 ± 0.71	2.89 ± 0.51	3.32 ± 1.07	2.77 ± 0.45	2.97 ± 1.14	2.99 ± 0.99	1.83 ± 2.04	2.09 ± 3.02	1.32 ± 0.43	1.38 ± 0.26
K	0.61 ± 0.06	0.43 ± 0.52	0.61 ± 0.07	0.46 ± 0.41	0.92 ± 0.17	0.35 ± 1.51	1.31 ± 0.39	1.13 ± 0.86	0.48 ± 3.03	0.29 ± 0.99
Model 3 (IVIM)										
D (10-3 mm^2/s)	1.51 ± 0.18	1.49 ± 0.14	1.32 ± 0.61	1.38 ± 0.22	0.91 ± 0.14	**1.02 ± 0.09***	0.82 ± 0.68	0.65 ± 0.06	0.86 ± 0.22	0.82 ± 0.23
Fp	0.37 ± 0.19	0.36 ± 0.11	0.39 ± 0.21	0.43 ± 0.17	0.33 ± 0.09	**0.28 ± 0.12***	0.19 ± 0.12	**0.11 ± 0.07***	0.24 ± 0.17	0.31 ± 0.19
D* (10-3 mm^2/s)	9.89 ± 5.19	6.91 ± 4.88	8.36 ± 3.67	6.72 ± 6.99	54.89 ± 35.74	99.74 ± 70.89	26.01 ± 28.42	19.09 ± 19.54	4.67 ± 4.74	3.11 ± 0.85
Model 4 (IVIM-DKI)										
D (10-3 mm^2/s)	2.37 ± 0.38	2.22 ± 0.41	2.43 ± 0.23	2.35 ± 0.24	1.21 ± 0.18	1.31 ± 0.23	1.23 ± 1.65	0.68 ± 0.29	1.41 ± 0.23	1.55 ± 0.24
Fp	0.15 ± 0.11	0.14 ± 0.12	0.15 ± 0.18	0.09 ± 0.06	0.27 ± 0.12	0.31 ± 0.23	0.13 ± 0.11	0.18 ± 0.14	0.03 ± 0.07	0.04 ± 0.12
D* (10-3 mm^2/s)	67.44 ± 112.33	39.79 ± 53.34	46.91 ± 51.85	56.32 ± 60.59	72.17 ± 48.86	136.13 ± 88.98	52.71 ± 57.45	45.08 ± 50.71	6.15 ± 10.11	4.51 ± 8.28
K	0.47 ± 0.07	0.41 ± 0.21	0.54 ± 0.11	0.47 ± 0.08	0.71 ± 0.31	0.61 ± 0.41	0.54 ± 0.74	0.02 ± 1.14	0.62 ± 0.69	0.77 ± 0.22

Statistical significances with $P < 0.05$ are bold and marked with *.

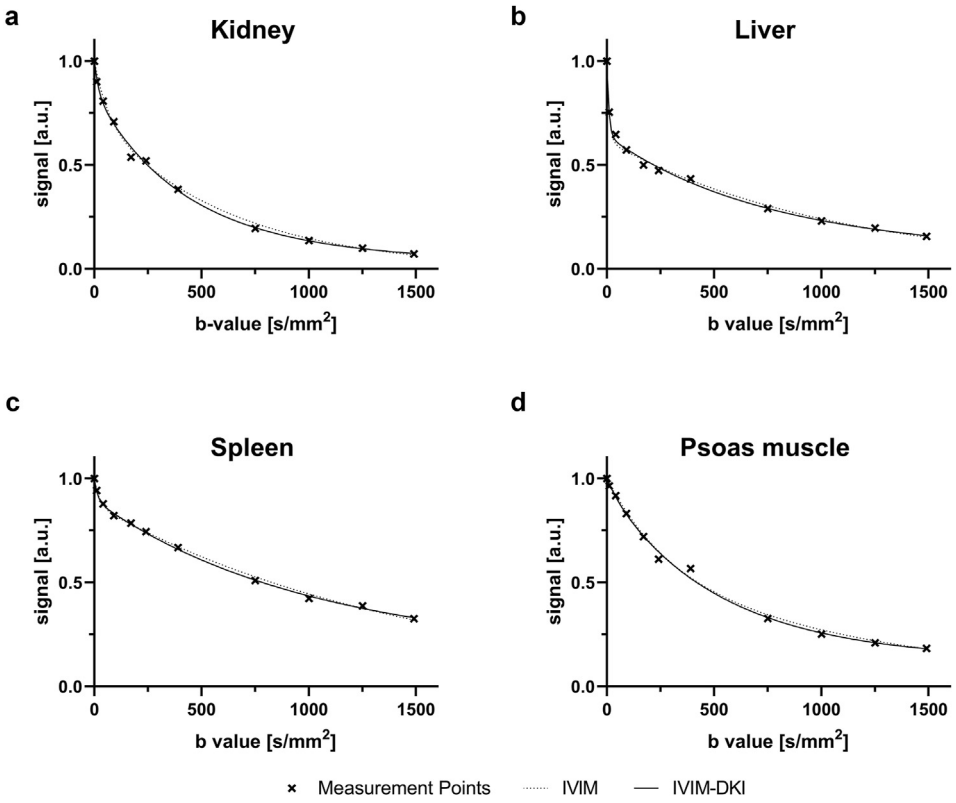

Figure 3. Typical IVIM-DKI and pure IVIM fitting curves before water challenge for: a) kidney cortex, b) liver, c) spleen, d) psoas muscle. The figures represent the average value of all volunteers.

Similarly, there were no statistically significant differences in diffusion parameters from the renal parenchyma, by means of all four models applied. In liver parenchyma, statistically significant changes where observed for the D value when applying the IVIM model ($p < 0.02$, Figure 5). *Fp* values significantly decreased after the water challenge in the liver and the spleen when assessed by the IVIM model ($p < 0.03$, Figure 6). K values after water challenge had a tendency to decrease in the renal, liver and the spleen parenchyma – however, without statistically significant effect. In the psoas muscle, the mean ADC value significantly increased after the water challenge ($p < 0.02$, Figure 7).

4. Discussion

The MRI diffusion signal of the kidneys is known to reflect not only the thermal-driven water diffusion but also mesoscopic fluid dynamics attributable to perfusion and tubular flow [16]. In healthy subjects, renal blood flow maintains the volume and composition of body fluids by adjusting the delivery of plasma filtered by the glomeruli. In our study, diffusion parameters calculated for all four models applied remained constant before and after water intake as observed for the renal parenchyma. This is in line with the compensatory mechanisms that are involved in homeostasis of body fluid composition. Moderate alterations in body hydration, as those induced in our study, are counterbalanced by the autoregulatory mechanisms of the renal blood flow, which is achieved by activation of several controlling mechanisms mainly acting on the diameter of the renal vasculature and involving the sympathetic nervous system, hormones and autacoids, and the renin–angiotensin system [17].

The results of our study also imply that the tissue hydration does not affect the robustness of the estimation of diffusion-related parameters in the kidneys. Therefore, it also does not affect the intra- and intersubject comparability of the diffusion parameters assessed using the applied models. This means, that even when applying highly sophisticated diffusion models, no special preparation regarding the hydration status is

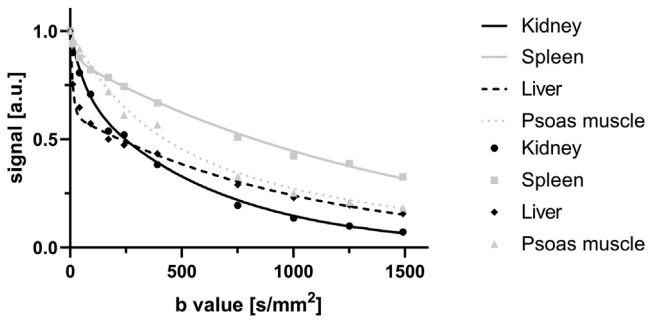

Figure 4. Typical IVIM_DKI fitting curves are shown before water challenge for kidney cortex, spleen, liver and psoas muscle. The figure represents the average value of all volunteers.

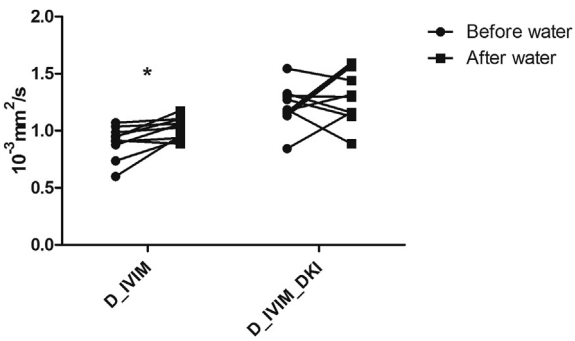

Figure 5. Typical behavior of the mean *D* values in the liver before and after water challenge when using both IVIM and IVIM_DKI models. The figure represents the average values of all volunteers.

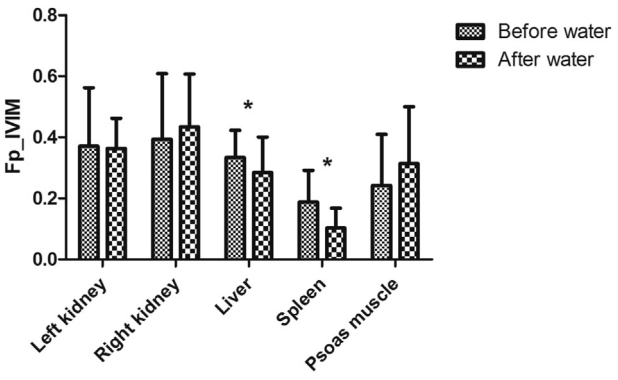

Figure 6. Typical behavior of the mean *Fp* values in various organs before and after water challenge. The figure represents the average values of all volunteers.

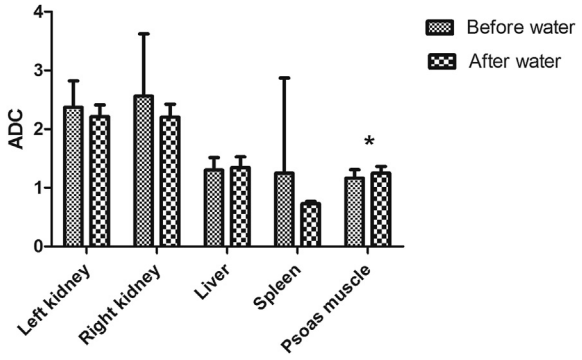

Figure 7. Typical behavior of the mean ADC values in various organs before and after water challenge. The figure represents the average values of all volunteers.

required. Although no change in diffusion values was found for the renal parenchyma, significant changes were observed in the liver, spleen and the skeletal muscle after the water challenge, which should be considered when diffusion values are compared between subjects with unknown hydration state.

Our IVIM analysis confirmed that effects of blood perfusion are pronounced in diffusion values from the liver [18]. Advanced diffusion methods such as IVIM and diffusion kurtosis may have potential for detection, staging and evaluation of the progression of various liver diseases, such as fibrosis and cirrhosis as well as in the characterization of focal liver lesions [19, 20]. In our study, both perfusion and water diffusion dependent parameters changed after the water challenge. It was previously showed, that portal venous flow increases 30 min after food intake, and the diffusion parameters obtained between fasting and food intake change less than 10% without reaching statistical significance [11]. Hence, we assume that water intake may increase portal venous flow as well, which might be the cause of the observed changes in the diffusion parameters. It might by hypothesized that the water intake could also be a factor for diffusion changes in the liver because water intake increases blood volume.

The highest DKI-K values before and after water challenge were seen in the spleen, possibly due to a more complex microstructure with a larger number of diffusion barriers causing water diffusion to deviate from a Gaussian distribution. We did not find significant differences in kurtosis parameters after water intake in abdominal parenchymal organs, which seems to be robust regarding water intake. Therefore, we believe that DKI may be considered a valuable technique for the detection of viable hepatocellular carcinoma (HCC) after radiofrequency ablation [21, 22]. Thus DKI values for different focal lesion types could be applicable independently of accompanying diffuse liver parenchyma alterations [22, 23, 24].

Previously reported diffusion parameters for the renal parenchyma, liver, spleen and psoas muscle in healthy volunteers are listed in Table 2. The values obtained in our study were univocal with to other studies, yet our study is more extended, with 4 different diffusion models applied before and after the water load [4, 8, 9, 14, 18, 20, 21, 23, 24]. In several previous studies [25, 26], a change of ADC values after changing the hydration state was reported. We were not able to reproduce these findings in spite of our successful hydration challenge, which caused significant changes in liver and spleen.

Our study has some limitations. First, a relatively low number of volunteers was included. Still, the obtained diffusion parameters were homogeneous within the group. The study cohort was large enough that several of the diffusion parameters showed significant differences in the liver, the spleen parenchyma and the skeletal muscle tissue after the water challenge whereas the diffusion parameters for the renal parenchyma remained stable. However, we cannot exclude that significant differences might be depicted in a larger study cohort, also in the kidneys. Second, the study was performed only at the magnetic field strength of 3T. In principle, the diffusion physiology and the describing diffusion parameters are independent of the field strength. However, due to the differences in MR scanner hardware and software, the MR diffusion parameters deviate between 1.5T and 3.0T in practice. Therefore, we cannot completely exclude that findings might be slightly different at 1.5T. Third, only healthy young volunteers have been included in this study. Therefore, we cannot confidently state, that our study results are transferable to all the patients of all ages and we cannot completely rule out whether the findings are still valid in the patients with diffuse diseases of the abdominal organs – especially in those diseases affecting the water homeostasis. Fourth, we assessed diffusion parameters only after a single physiological challenge – an oral water administration -, but we did not investigate food intake or the effect of medications affecting water homeostasis such as diuretics. Fifth, there was no voxelwise estimation of diffusion indices performed in our study and the reason for first averaging the ROIs and subsequently performing the exponential fit is the instability of IVIM fitting parameters and particularly of the perfusion related parameters, which strongly increases with lower SNR. In our experience, the fit instability is much higher as compared to image noise. Fit stability can be improved by increasing the SNR of the DWI images using (a) a higher number of averages increasing acquisition time, or (b) applying filter techniques reducing spatial resolution. Our choice was a compromise to allow for stable curve fitting using a DWI sequence with clinically feasible acquisition time and reasonable spatial resolution. Sixth, the number of averages of diffusion images was increased for higher b-values to keep SNR at a sufficient level even for high b-values. Acquiring the same number of averages for all b-values would have led to inacceptable acquisition times. Therefore, we cannot exclude that the number of averages per b-values might have influenced the evaluation. Seventh, kidneys, liver, spleen and psoas muscle present rather different diffusion properties, as shown/confirmed also in Table 1. While optimal b-values for estimating diffusion indices depend on diffusion properties of a tissue, in the present study the same set of b-values was used for all tissues. Eighth, we did not investigate the known effects of diffusion anisotropy on IVIM and DKI models, which was out of the scope of this study. The use of trace-weighted images is; therefore, one of the limitations of the study [27, 28]. Ninth, we did not check the correct application of diffusion gradients in the DWI sequence, which might have influenced calculated parameters [29, 30]. Finally, due to small study cohort, an intra-patient variability was not evaluated. Therefore, it is unknown whether the effect of the change in hydration state is actually larger or equal than the repeatability of the diffusion parameters estimated. Still, the main finding of our study shows stability of the diffusion parameters calculated for the renal parenchyma, in spite of induced body hydration changes. Hence, these findings are in the order of the repeatability error. In the other organs as the liver, the spleen parenchyma and the skeletal muscle, we were able to detect statistically significant changes between the two hydration states.

Table 2. Comparison of the parameters of the intravoxel incoherent motion (IVIM), diffusion kurtosis (DKI) and combined IVIM-DKI imaging models before (B/w) and after (A/w) water administration obtained in our study and in the previous studies. Means and standard deviations for the region of interest (ROI) analysis over all subjects are shown.

	Kidney parenchyma b/w	Liver b/w	Spleen b/w	Psoas muscle b/w
DWI-ADC (10^{-3} mm^2/s)				
Current study ($n = 10$)	2.37 ± 0.45	1.31 ± 0.21	1.25 ± 1.63	1.16 ± 0.14
Cercueil JP et al ($n = 36$) [23]		1.72 ± 0.04		
Sulkowska K et al ($n = 35$) [9]	2.05			
Wyttenbach R et al ($n = 40$) [20]		1.83 ± 0.44		
Perrone N et al ($n = 10$) [21]	3.00 ± 0.42			
Wurnig MC et al ($n = 8$) [14]	2.52 ± 0.79	4.88 ± 3.58	0.83 ± 0.18	1.77 ± 0.36
Hayashi T et al ($n = 10$) [18]		1.32 ± 0.13		
DKI-D (10^{-3} mm^2/s)				
Current study ($n = 10$)	3.22 ± 0.71	2.97 ± 1.14	1.83 ± 2.04	1.32 ± 0.43
Wurnig MC et al ($n = 8$) [14]	3.11 ± 0.75	4.22 ± 1.80	1.67 ± 0.75	2.37 ± 0.65
DKI-K				
Current study ($n = 10$)	0.61 ± 0.06	0.92 ± 0.17	1.31 ± 0.39	0.48 ± 3.03
Wurnig MC et al ($n = 8$) [14]	0.80 ± 0.18	1.04 ± 0.25	1.72 ± 0.32	0.93 ± 0.25
IVIM-D (10^{-3} mm^2/s)				
Current study ($n = 10$)	1.51 ± 0.18	0.91 ± 0.14	0.82 ± 0.68	0.86 ± 0.22
Wurnig MC et al ($n = 8$) [4]	1.72	1.16		
Sulkowska K et al ($n = 35$) [9]	1.85			
Lemke A et al ($n = 3$) [8]	1.56 ± 0.20	1.00 ± 0.05	0.67 ± 0.02	
Kuai ZX et al ($n = 150$) [24]	1.74 ± 0.02	1.21 ± 0.02	0.75 ± 0.04	
Wyttenbach R et al ($n = 40$) [20]		1.05 ± 0.11		
Hayashi T et al ($n = 10$) [18]		1.03 ± 0.05		
IVIM-Fp				
Current study ($n = 10$)	0.37 ± 0.19	0.33 ± 0.09	0.19 ± 0.12	0.24 ± 0.17
Wurnig MC et al ($n = 8$) [4]	0.303	0.229		
Kuai ZX et al ($n = 150$) [24]	0.73 ± 0.01	0.66 ± 0.02	0.83 ± 0.02	
IVIM-D* (10^{-3} mm^2/s)				
Current study ($n = 10$)	9.89 ± 5.19	54.89 ± 35.74	26.01 ± 28.42	4.67 ± 4.74
Wurnig MC et al ($n = 8$) [4]	11.8	65.5		
Lemke A et al ($n = 3$) [8]	43 ± 24	78 ± 42	90 ± 53	
Kuai ZX et al ($n = 150$) [24]	13.07 ± 0.82	19.32 ± 0.94	12.31 ± 1.02	
Wyttenbach R et al ($n = 40$) [20]		40.7 ± 19.9		
Hayashi T et al ($n = 10$) [18]		29.47 ± 5.47		
IVIM-DKI-D (10^{-3} mm^2/s)				
Current study ($n = 10$)	2.37 ± 0.38	1.21 ± 0.18	1.23 ± 1.65	1.41 ± 0.23
Cercueil JP et al ($n = 36$) [23]		1.50 ± 0.03		
Wurnig MC et al ($n = 8$) [4]	2.8	1.53		
IVIM-DKI-Fp				
Current study ($n = 10$)	0.15 ± 0.11	0.27 ± 0.12	0.13 ± 0.11	0.03 ± 0.07
Wurnig MC et al ($n = 8$) [4]	0.125	0.192		
IVIM-DKI-D* (10^{-3} mm^2/s)				
Current study ($n = 10$)	67.44 ± 112.33	72.17 ± 48.86	52.71 ± 57.45	6.15 ± 10.11
Wurnig MC et al ($n = 8$) [4]	56.3	103.3		

Therefore, it is clear that the variations found are higher than the intra-patient variability.

From the perspective of signal acquisition and statistical evaluation, we tried to provide accuracy to our approach along with keeping the signal quality at high b-values. This was important for further comparison of calculated diffusion values, coming from the same patients in two hydration states. Subsequently, we applied a paired two-sample two-tailed t-test for statistical evaluation of diffusion parameters from two hydration states. Although the number of subjects would indicate application of nonparametric test for comparison of diffusion parameters coming from less than 20 subjects, Shapiro-Wilk normality test did not reject all the calculated distributions of diffusion parameters from normality. Moreover, application of for instance Wilcoxon signed-rank test would provide us the information on rather how the medians of diffusion parameters distributions are far from each other, instead of focusing on their mean values. Furthermore, nonparametric test would be prone to reject even smallest true positive effects, treating those as a false positive findings at the cost of reduced sensitivity to small changes appearing between two hydration states.

Finally, we would also like to highlight that in the future studies, a novel technique of ^{23}Na -MRI may contribute to the quantification of indexes relevant in the fluid volume regulation and in the characterization of renal functional mechanisms involved. It was recently shown that sodium MRI has the ability to provide information on the glomerular filtration in kidneys by means of the cortico-medullary gradient in physiological and pathophysiological conditions [31, 32, 33]. Hence, further research on combining diffusion-weighted ^{1}H-MRI and ^{23}Na-MRI

is desirable [34, 35], including assessment of the physiological changes in sodium body content [36, 37].

5. Conclusions

We demonstrated that diffusion parameters calculated from the renal parenchyma remain remarkably stable independently from body hydration level or the applied diffusion model. This may be assigned to the renal autoregulatory compensation mechanisms. However, diffusion parameters in the liver, the spleen parenchyma and the psoas muscle showed to be sensitive to the change in body hydration induced by the water challenge. The findings of our study suggest that the hydration state does not to be considered in diffusion MRI of the kidneys, whereas in the liver, spleen, and the skeletal muscles a standardized preparation of the patient before the MRI examination should be taken into account if diffusion data is acquired.

Declarations

Author contribution statement

J. Kemėšienė and A. Rühle: Performed the experiments; Analyzed and interpreted the data; Wrote the paper.

R. Gomolka: Analyzed and interpreted the data; Contributed reagents, materials, analysis tools or data; Wrote the paper.

M. Wurnig: Conceived and designed the experiments; Contributed reagents, materials, analysis tools or data.

C. Rossi: Conceived and designed the experiments; Wrote the paper.

A. Boss: Conceived and designed the experiments; Analyzed and interpreted the data; Contributed reagents, materials, analysis tools or data; Wrote the paper.

Funding statement

This work was supported by the Clinical Research Priority Program of the University of Zurich for the CRPP Hypertension Research Network (HYRENE).

Declaration of interests statement

The authors declare no conflict of interest.

Additional information

No additional information is available for this paper.

Acknowledgements

We would like to thank Dr. Markus Klarhoefer from Siemens Healthcare AG for his support during protocol optimization.

This work was supported by the Clinical Research Priority Program of the University of Zurich for the CRPP Hypertension Research Network (HYRENE).

References

[1] F. Artunc, C. Rossi, A. Boss, MRI to assess renal structure and function, Curr. Opin. Nephrol. Hypertens. 20 (6) (2011) 669–675.
[2] J.L. Zhang, H. Rusinek, H. Chandarana, V.S. Lee, Functional MRI of the kidneys, J. Magn. Reson. Imag. 37 (2) (2013) 282–293.
[3] J.-P. Vallée, A. Ljimani, P. Boor, L. Gullapudi, N.M. Selby, M. Notohamiprodjo, et al., Diffusion-weighted magnetic resonance imaging to assess diffuse renal pathology: a systematic review and statement paper, Nephrol. Dial. Transplant. 33 (2) (2018) 29–40.
[4] M.C. Wurnig, M. Germann, A. Boss, Is there evidence for more than two diffusion components in abdominal organs? – a magnetic resonance imaging study in healthy volunteers, NMR Biomed. 31 (1) (2018) 1–9.
[5] D. Le Bihan, E. Breton, D. Lallemand, L.M. Aubin, J. Vignaud, M. Laval-Jeanet, Separation of diffusion and perfusion in intravoxel incoherent motion MR imaging, Tep Apx. 60 (8) (1988) 27–30.
[6] H. Schmidt, S. Gatidis, P. Martirosian, Impact of measurement parameters on apparent diffusion coefficient quantification in diffusion-weighted-magnetic resonance imaging, Invest. Radiol. 50 (1) (2015) 46–56.
[7] D. Le Bihan, What can we see with IVIM MRI? Neuroimage 15 (2) (2019) 56–57.
[8] A. Lemke, B. Stieltjes, L.R. Schad, F.B. Laun, Toward an optimal distribution of b values for intravoxel incoherent motion imaging, Magn. Reson. Imaging 29 (6) (2011) 766–776.
[9] K. Sulkowska, P. Palczewski, D. Wojcik, M. Ciszek, J. Sanko-Resmer, J. Wojtowicz, et al., Intravoxel incoherent motion imaging in monitoring the function of kidney allograft, Acta Radiol. 60 (7) (2019) 925–932.
[10] W.C. Huang, B. Gaing, H. Chandarana, N.S. Parikh, E.E. Sigmund, D. Stoffel, et al., Subtype differentiation of renal tumors using voxel-based histogram analysis of intravoxel incoherent motion parameters, Invest. Radiol. 50 (3) (2014) 144–152.
[11] S. Pazahr, D. Nanz, C. Rossi, N. Chuck, I. Stenger, M.C. Wurnig, F. Schick, A. Boss, Magnetic resonance imaging of the liver : apparent diffusion coefficients from multiexponential analysis of b values greater than 50 s/mm2 do not respond to caloric intake despite increased portal-venous blood flow, Invest. Radiol. 49 (3) (2014) 138–146.
[12] L. Yan, C. Liang, X. Chen, Z. Liu, Z. Zhang, D. Pan, et al., MRI quantification of non-Gaussian water diffusion in normal human kidney: a diffusional kurtosis imaging study, NMR Biomed. 28 (2) (2014) 154–161.
[13] J.H. Jensen, J.A. Helpern, A. Ramani, H. Lu, K. Kaczynski, Diffusional kurtosis imaging: the quantification of non-Gaussian water diffusion by means of magnetic resonance imaging, Magn. Reson. Med. 53 (6) (2005) 1432–1440.
[14] M.C. Wurnig, D. Kenkel, L. Filli, A. Boss, A standardized parameter-free algorithm for combined intravoxel incoherent motion and diffusion kurtosis analysis of diffusion imaging data, Invest. Radiol. 51 (3) (2016) 203–210.
[15] M.C. Wurnig, O.F. Donati, E. Ulbrich, L. Filli, D. Kenkel, H.C. Thoeny, et al., Systematic analysis of the intravoxel incoherent motion threshold separating perfusion and diffusion effects: proposal of a standardized algorithm, Magn. Reson. Med. 74 (5) (2015) 1414–1422.
[16] M. Notohamiprodjo, H. Chandarana, A. Mikheev, H. Rusinek, J. Grinstead, T. Feiweier, et al., Combined intravoxel incoherent motion and diffusion tensor imaging of renal diffusion and flow anisotropy, Magn. Reson. Med. 73 (4) (2015) 1526–1532.
[17] S.J. Enna, D.B. Bylund, The Comprehensive Pharmacology Reference, 2008.
[18] T. Hayashi, T. Miyati, J. Takahashi, K. Fukuzawa, H. Sakai, M. Tano, et al., Diffusion analysis with triexponential function in liver cirrhosis, J. Magn. Reson. Imag. 38 (1) (2013) 148–153.
[19] S. Lewis, D. Hadrien, Y. Cui, B. Taouli, Diffusion-weighted imaging of the liver: techniques and applications, Magn. Reson. Imag. Clin. N. Am. 22 (3) (2014) 373–395.
[20] R. Wyttenbach, S. Colagrande, B. Matteuzzi, P. Santini, S. Busoni, F. Regini, et al., Assessment of liver perfusion by IntraVoxel incoherent motion (IVIM) magnetic resonance–diffusion-weighted imaging, J. Comput. Assist. Tomogr. 39 (3) (2015) 365–372.
[21] N. Perrone, R. Pontremoli, A. Tagliafico, M.B. Damasio, C. Tomolillo, L.E. Derchi, et al., Diffusion-weighted MRI sequences (DW-MRI) of the kidney: normal findings, influence of hydration state and repeatability of results, Radiol. Med. 113 (2) (2008) 214–224.
[22] J. Budjan, E.A. Sauter, F.G. Zoellner, A. Lemke, J. Wambsganss, S.O. Schoenberg, et al., Diffusion kurtosis imaging of the liver at 3 Tesla: in vivo comparison to standard diffusion-weighted imaging, Acta Radiol. 59 (1) (2018) 18–25.
[23] J.P. Cercueil, J.M. Petit, S. Nougaret, Ph Soyer, A. Fohen, et al., Intravoxel incoherent motion diffusion-weighted imaging in the liver: comparison of mono-, bi- and tri-exponential modelling t 3, 0T. European Radiology 25 (6) (2014) 1541–1550.
[24] Z.C. Kuai, W.Y. Liu, Y.M. Zhu, Effect of multiple perfusion components on pseudo-diffusion coefficient in intravoxel incoherent motion imaging, Phys. Med. Biol. 62 (21) (2017) 8197–8209.
[25] E.E. Sigmund, P.H. Vivier, D. Sui, N.A. Lamparello, K. Tantillo, A. Mikheev, H. Rusinek, J.S. Babb, P. Storey, V.S. Lee, H. Chandarana, Intravoxel incoherent motion and diffusion-tensor imaging in renal tissue under hydration and furosemide flow challenges, Radiol. 263 (3) (2012) 758–769.
[26] M.B. Damasio, A. Tagliafico, E. Capaccio, C. Cancelli, N. Perrone, C. Tomolillo, R. Pontremoli, L.E. Derchi, Diffusion-weighted MRI sequences (DW-MRI) of the kidney: normal findings, influence of hydration state and repeatability of results, Radiol. Med. 113 (2) (2008) 214–224.
[27] T. Finkenstaedt, M. Klarhoefer, C. Eberhardt, A.S. Becker, G. Andreisek, A. Boss, C. Rossi, The IVIM signal in the healthy cerebral gray matter: a play of spherical and non-spherical components, Neuroimage 15 (152) (2017) 340–347.
[28] M. Giannelli, N. Toschi, On the use of trace-weighted images in body diffusional kurtosis imaging, Magn. Reson. Imaging 34 (4) (2016) 502–507.
[29] D.K. Jones, Precision and accuracy in diffusion tensor magnetic resonance imaging, Top. Magn. Reson. Imag. 21 (2) (2010) 87–99.
[30] Fedeli, et al., Dependence of apparent diffusion coefficient measurement on diffusion gradient direction and spatial position - a quality assurance intercomparison study of forty-four scanners for quantitative diffusion-weighted imaging, Phys. Med. 55 (11) (2018) 135–141.
[31] N. Maril, R. Margalit, J. Mispelter, H. Degani, Sodium magnetic resonance imaging of diuresis: spatial and kinetic response, Magn. Reson. Med. 53 (3) (2005) 545–552.
[32] N. Maril, Y. Rosen, G.H. Reynolds, A. Ivanishev, L. Ngo, R.E. Lenkinski, Sodium MRI of the human kidney at 3 tesla, Magn. Reson. Med. 56 (6) (2006) 1229–1234.

[33] S. Haneder, S. Konstandin, J.N. Morelli, A.M. Nagel, F.G. Zoellner, H.J. Michaely, 23Na MR imaging of the human kidneys at 3 T : before and after a water load, Radiology 260 (3) (2011) 857–865.
[34] S. Haneder, P. Kettnaker, S. Konstandin, J.N. Morelli, L.R. Schad, S.O. Schoenberg, et al., Quantitative in vivo 23Na MR imaging of the healthy human kidney: determination of physiological ranges at 3.0T with comparison to DWI and BOLD. Magn Reson Mater Physics, Biol. Med. 26 (6) (2013) 501–509.
[35] D. Hausmann, S. Konstandin, F. Wetterling, S. Haneder, A.M. Nagel, D.J. Dinter, et al., Apparent diffusion coefficient and sodium concentration measurements in human prostate tissue via hydrogen-1 and sodium-23 magnetic resonance imaging in a clinical setting at 3 T, Invest. Radiol. 47 (12) (2012) 677–682.
[36] J. Titze, Sodium balance is not just a renal affair, Curr. Opin. Nephrol. Hypertens. 23 (2) (2014) 101–105.
[37] L.H. Hofmeister, S. Perisic, J. Titze, Tissue sodium storage: evidence for kidney-like extrarenal countercurrent systems? Pflugers Arch Eur J Physiol 467 (3) (2015) 551–558.